

Porous Silicon Nanoparticle Photosensitizers for Singlet Oxygen and Their Phototoxicity against Cancer Cells

Ling Xiao,[†] Luo Gu,[‡] Stephen B. Howell,[§] and Michael J. Sailor^{‡,*}

[†]Department of Chemistry and Biochemistry, University of California, San Diego, 9500 Gilman Drive, La Jolla, California 92093-0358, United States, [‡]College of Life Science and Technology, Huazhong University of Science and Technology, Wuhan, P.R. China, and [§]Department of Medicine and the Moores UCSD, Cancer Center, University of California, San Diego, 3855 Health Sciences Drive, La Jolla, California 92093-0819, United States

Photodynamic therapy (PDT) can be an effective clinical treatment for certain types of cancer because of its relatively low systemic toxicity and its noninvasive nature.¹ The operational principle for PDT involves the conversion of ground-state molecular oxygen (³O₂) to singlet oxygen (¹O₂) by energy transfer from a photoexcited molecule (a photosensitizer). The highly reactive ¹O₂ causes lethal damage to cancer cells and destruction of tumor vasculature.^{2,3} Despite the advantages of the therapy itself, photosensitizers in use today display toxic or other side effects that limit their use. For example, the first-generation photosensitizer Photofrin lacks a long wavelength absorption band and it exhibits prolonged residence time in the normal tissues of the body. If not protected from sunlight and other forms of bright light, the skin and eyes of the patient can become severely damaged. It takes only a few minutes of exposure to induce a light sensitivity response, and this sensitivity can persist for 4–12 weeks after administration of the therapeutic.⁴ More promising second-generation photosensitizers, such as Photosens, are based on a phthalocyanine motif with a strong long wavelength absorption band. However, most phthalocyanines and their relatives are hydrophobic, requiring delivery systems for clinical use,^{5,6} and patient photosensitivity remains a problem.⁷ Third-generation photosensitizers involve second-generation photosensitizers modified with targeting molecules for better tumor selectivity.⁸

Recent studies using nanoparticle hosts containing conventional organic photosensitizers have demonstrated improved water

ABSTRACT Porous Si nanoparticles, prepared from electrochemically etched single crystal Si wafers, function as photosensitizers to generate ¹O₂ in ethanol and in aqueous media. The preparation conditions for the porous Si nanoparticles were optimized to maximize (1) the yield of material; (2) its quantum yield of ¹O₂ production; and (3) its *in vitro* degradation properties. The optimal formulation was determined to consist of nanoparticles 146 ± 7 nm in diameter, with nominal pore sizes of 12 ± 4 nm. The quantum yield for ¹O₂ production is 0.10 ± 0.02 in ethanol and 0.17 ± 0.01 in H₂O. HeLa or NIH-3T3 cells treated with 100 μg/mL porous Si nanoparticles and exposed to 60 J/cm² white light (infrared filtered, 100 mW/cm² for 10 min) exhibit ~45% cell death, while controls containing no nanoparticles show 10% or 25% cell death, respectively. The dark control experiment yields <10% cytotoxicity for either cell type.

KEYWORDS: porous silicon · nanoparticles · photodynamic therapy · photosensitizer · singlet oxygen

solubility and biocompatibility.^{9–15} However, most of these approaches use nonfunctional silica or polymer-based nanomaterials as the carriers, and there is still a risk of the photosensitizer payload leaking from the carriers into the body before reaching the target. Nanomaterials that can intrinsically generate ¹O₂ when photoexcited, such as TiO₂^{16,17} and quantum dots,^{18,19} can overcome such problems. However, concerns regarding biodegradability,²⁰ toxicity of degradation byproduct,^{21–24} and relatively low ¹O₂ quantum yield¹⁸ of such materials have impeded their clinical application.

It has been recently discovered that the quantum-confined domains in porous Si films can generate ¹O₂ when excited with visible light, and this energy transfer process is very efficient due to the extremely long lifetime of the excitons and the large specific surface area of porous Si.^{25,26} Porous Si has low toxicity, and most importantly, it is biodegradable and biocompatible.^{27–31}

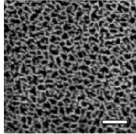
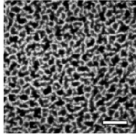
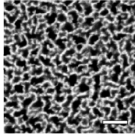
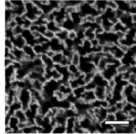
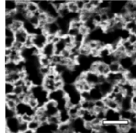
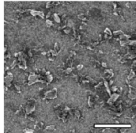
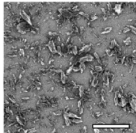
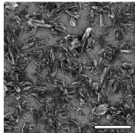
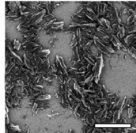
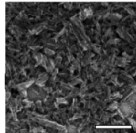
* Address correspondence to msailor@ucsd.edu.

Received for review December 19, 2010 and accepted March 31, 2011.

Published online March 31, 2011
10.1021/nn1035262

© 2011 American Chemical Society

TABLE 1. Characteristics of Porous Si Nanoparticles (PSiNP) Prepared with Different Etching Current Densities

	50 mA/cm ²	100 mA/cm ²	200 mA/cm ²	300 mA/cm ²	400 mA/cm ²
PSiNP size (nm) ^[a]	109.7 ± 11.6	129.6 ± 5.5	146.4 ± 6.6	170.5 ± 4.3	157.8 ± 1.5
Pore size (nm) ^[b]	7.9 ± 2.9	9.2 ± 1.8	11.8 ± 3.8	13.1 ± 5.1	17.9 ± 9.3
Pore ^[c]					
PSiNP ^[d]					
$\Phi_{\text{PSiNP}}^{\text{[e]}}$	0.07 ± 0.02	0.12 ± 0.03	0.10 ± 0.02	0.05 ± 0.01	0.05 ± 0.01

^a PSiNP size (nm) represents the average hydrodynamic size measured by DLS. ^b Pore size (nm) represents the average pore size of the freestanding film measured by SEM. ^c Plan-view images of freestanding porous Si films, showing the pore morphology scale bar is 50 nm. ^d Morphology of porous Si nanoparticles prepared from the films in panels c. Scale bar is 1 μm . ^e $^1\text{O}_2$ quantum yield of the porous Si nanoparticles.

Silicon is a common trace element in humans and the primary biodegradation product of porous Si, orthosilicic acid ($\text{Si}(\text{OH})_4$), is the form predominantly absorbed by humans and is naturally present in numerous tissues.^{32–34} We have previously found that porous Si nanoparticles administered *in vivo* (mouse model) can accumulate in tumors and then degrade into components that are rapidly cleared by the kidneys in a relatively short period of time.³⁵ In this study, we show that porous Si nanoparticles can generate $^1\text{O}_2$ and kill cancer cells *in vitro* following illumination with a commercial halogen light or a light-emitting diode (LED) panel. This study represents the first *in vitro* demonstration of photodynamic killing of cancer cells using porous Si nanoparticles, and it illustrates the potential for this nanomaterial as a nontoxic, biodegradable alternative to molecular PDT agents used in the clinic today.

RESULTS AND DISCUSSION

Porous Si nanoparticles were prepared by electrochemical etching of single-crystal silicon wafers in ethanolic HF solution, lift-off the porous Si film, ultrasonication, and finally filtration of the formed particles through a 0.45 μm membrane (Supporting Information, Scheme S1). To study the effect of the pore size in the nanoparticles on the generation of singlet oxygen, porous Si nanoparticles with different average pore sizes (7.9–17.6 nm) were prepared by using various etching current densities from 50 to 400 mA/cm² (Table 1). The as-prepared nanoparticles possess a hydrogen-terminated surface (Supporting Information, Figure S1), and their average hydrodynamic size measured by dynamic light scattering (DLS) is ~ 100 to

200 nm. Scanning electron microscope (SEM) images reveal a well-ordered mesoporous nanostructure (Table 1).

The generation of $^1\text{O}_2$ by photoexcited porous Si nanoparticles in ethanol was detected using the chemical trapping reagent 1,3-diphenylisobenzofuran (DPBF). DPBF reacts with $^1\text{O}_2$ irreversibly, undergoing a 1,4-cycloaddition that is detected as a decrease in the intensity of the DPBF absorption band at 410 nm.^{36,37} As shown in Figure 1a, the absorption intensity of the solution containing porous Si nanoparticles and DPBF decreases gradually as a function of time under light irradiation (halogen lamp fitted with an IR filter and a 454–500 nm bandpass filter), while the change is negligibly small in the absence of light (Figure 1b). DPBF was observed to undergo slight decomposition under the irradiation conditions (in air), even in the absence of porous Si nanoparticles (Supporting Information, Figure S2). The data presented here are corrected for this self-photobleaching. To confirm that the decomposition of DPBF is caused by $^1\text{O}_2$ instead of a direct reaction with photoexcited porous Si nanoparticles, the photolysis reaction was carried out in a solution depleted of O_2 (by N_2 purge for 30 min). The decrease of the absorption of DPBF in O_2 -depleted solution was negligible compared to that of the air-saturated solution (Figure 1d). The dependence of the reaction on dissolved O_2 provides clear evidence that $^1\text{O}_2$ is generated by the porous Si nanoparticles in the photosensitized process. The photosensitization reaction accelerates with increasing nanoparticle concentration (Supporting Information, Figure S3).

The quantum yield for $^1\text{O}_2$ generation by porous Si nanoparticles was determined using a comparative

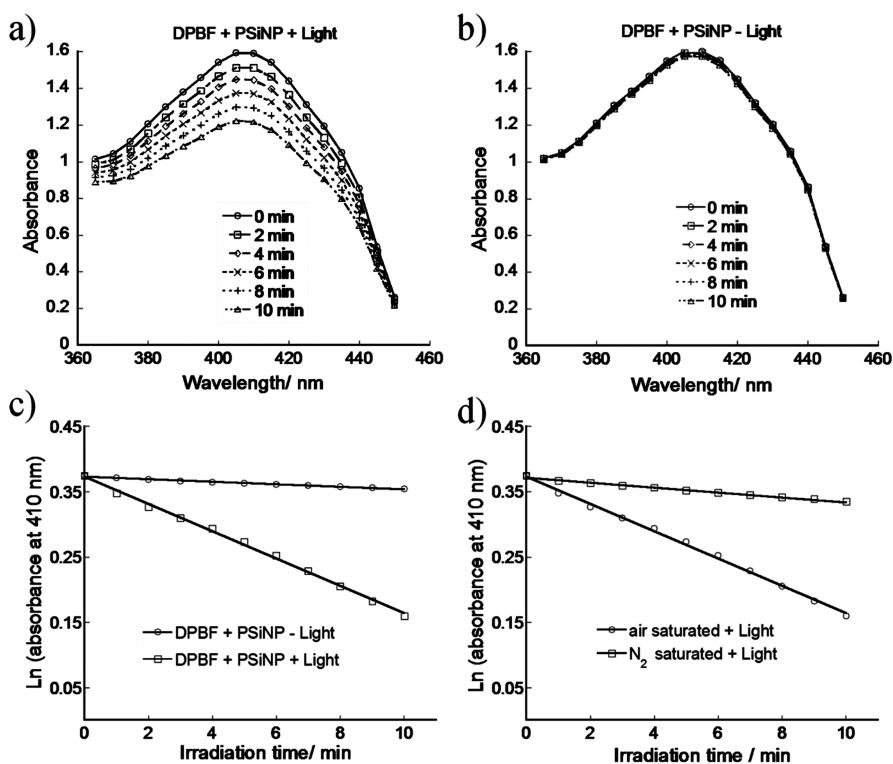


Figure 1. Time course of the absorption spectrum of the singlet oxygen indicator DPBF with porous Si nanoparticles (PSiNP) (a) in the presence of and (b) in the absence of light. Solution measurements were obtained in air-saturated ethanol. (c) Decay curves of the (background-corrected) 410-nm absorption bands from (a) and (b). (d) Decay curves of the (background-corrected) 410-nm absorption band from DPBF in irradiated solutions containing PSiNP, in either air-saturated or N_2 -saturated solutions.

method.³⁸ A plot of optical absorbance at 410 nm as a function of irradiation time is consistent with a first order reaction (Figure 1c). The 1O_2 quantum yield was calculated by comparison with a standard photosensitizer,³⁹

$$\Phi_{\text{PSiNP}} = \Phi_s \frac{k_{\text{PSiNP}} I_s}{I_{\text{PSiNP}} k_s} \quad (1)$$

where k_{PSiNP} and k_s are the rate constants for decomposition of DPBF by porous Si nanoparticles and by a standard photosensitizer, respectively. I_{PSiNP} and I_s represent light absorbed by the porous Si nanoparticles and by the photosensitizer standard, respectively, which are determined by integration of the optical absorption bands in the wavelength range 454–500 nm. To evaluate the method and our experimental setup, the 1O_2 quantum yield of methylene blue (MB) was determined to be 0.53 using rose bengal (RB, $\Phi_{\text{RB}} = 0.86$ in ethanol⁴⁰) as a standard, which is in good agreement with the published data ($\Phi_{\text{MB}} = 0.52$ in ethanol⁴⁰). Similarly, by taking RB as a standard, the 1O_2 quantum yield of the porous Si nanoparticles as a function of average pore size was determined. As reported in Table 1, the intermediate pore size of 9.2–11.8 nm appears to be optimal for 1O_2 generation. In the present study, nanoparticles made using an etching current density of 200 mA/cm² were chosen for the *in vitro* tests, because this preparation provided

a compromise between maximizing the total yield of nanoparticles and maximizing the 1O_2 quantum yield.

Singlet oxygen generation by porous Si has been studied,²⁶ and it is thought to undergo the following processes: (1) porous Si is photoexcited into a singlet energy state; (2) the material undergoes intersystem crossing to a long-lived triplet state; (3) energy transfer from the excited triplet state on porous Si to the triplet ground state of oxygen (3O_2), generating singlet oxygen (1O_2). The 1O_2 excited state can then relax back to the ground state 3O_2 via radiative or nonradiative (collisional) deactivation.²⁶ For gas-phase oxygen, the efficiency of 1O_2 generation has been reported to increase with increasing porosity of the porous Si film.⁴¹ Moreover, for gas-phase oxygen the radiative deexcitation route dominates, while nonradiative relaxation is the main relaxation pathway for 1O_2 in solution.⁴² In the present work, no specific dependence of 1O_2 quantum yield on porosity was observed. This is attributed to the process by which the nanoparticles are prepared; ultrasonic fracture of the porous Si film into particles changes the pore morphology and it generates fresh reactive surfaces that are readily oxidized. The degree of oxidation is dependent on pore size,⁴³ and surface oxides may enhance nonradiative pathways and hinder triplet–triplet energy transfer.⁴⁴

The concentration of 1O_2 in aqueous solution was further quantified using singlet oxygen sensor green

(SOSG) reagent, which is highly selective for $^1\text{O}_2$ and does not have any appreciable response to hydroxyl radical ($\cdot\text{OH}$) or superoxide ($\cdot\text{O}_2^-$) species.⁴⁵ In the presence of $^1\text{O}_2$, SOSG emits strong green fluorescence (excitation/emission maxima $\sim 504/525$ nm), which corresponds to the formation of an endoperoxide by the reaction of $^1\text{O}_2$ with the anthracene component of SOSG.⁴⁶ When the assay solution containing porous Si nanoparticles was irradiated with light from a tungsten halogen lamp (filtered through a short pass infrared and a 454–500 nm bandpass filters), the fluorescence emission intensity at 520 nm was observed to increase gradually (Supporting Information, Figure S4a). An equivalent sample maintained in the dark showed no increase in fluorescence signal (Supporting Information, Figure S4b). The rate of SOSG endoperoxide formation followed first order kinetics (Figure 2),⁴⁷ and the quantum yield for $^1\text{O}_2$ generation by porous Si nanoparticles in water was determined to be 0.17 ± 0.01 using eq 1 (relative to $\Phi_{\text{RB}} = 0.75$ in H_2O ⁴⁰).

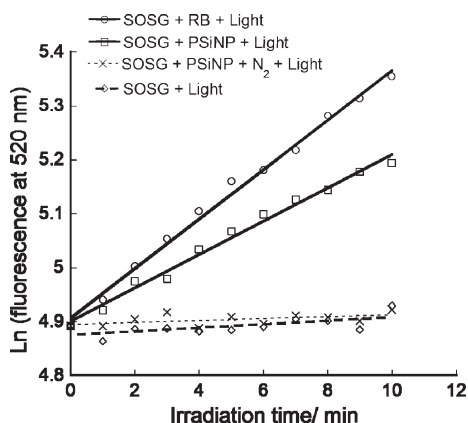


Figure 2. Increase in fluorescence intensity of SOSG endoperoxide as a function of irradiation time in the presence of SOSG alone, SOSG with RB, and SOSG with porous Si nanoparticles (PSiNP) in air and in N_2 saturated solution, respectively.

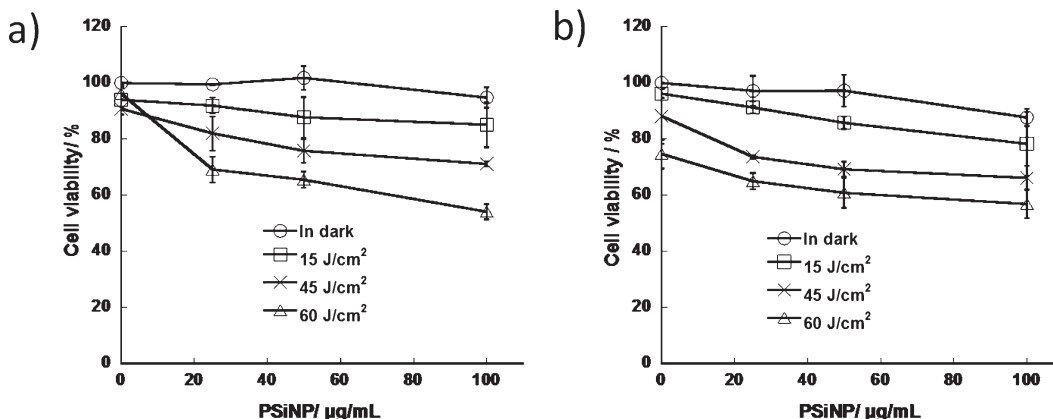


Figure 3. Photoinduced toxicity exhibited by (a) HeLa cells and (b) NIH-3T3 cells treated with porous Si nanoparticles. The medium containing the porous Si nanoparticles (PBS buffer) was replaced with cell growth medium (RPMI-1640 medium supplemented with 10% FBS) immediately after irradiation. Cell viability quantified by MTS assay. Illumination was accomplished with a (IR filtered) halogen lamp. Each data point represents the mean of three independent experiments.

In support of the conclusion that the observed signal was due to $^1\text{O}_2$ generation from photoexcited porous Si nanoparticles, no increase in fluorescence was observed for an irradiated sample that had been deoxygenated (by sparging with nitrogen gas for 30 min), or that contained SOSG alone (no nanoparticles, Figure 2).

The phototoxicity of porous Si nanoparticles toward cancer cells was tested *in vitro* using the MTS (3-(4,5-dimethylthiazol-2-yl)-5-(3-carboxymethoxyphenyl)-2-(4-sulfophenyl)-2H-tetrazolium) cell viability assay. HeLa and NIH-3T3 cells were irradiated for 10 min in a PBS buffer containing 0, 25, 50, and 100 $\mu\text{g}/\text{mL}$ porous Si nanoparticles. As shown in Figure 3, cell viability decreased with increasing concentration of porous Si nanoparticles and with increasing light intensity for both cell types studied. The maximum degree of cell death observed with the experimental protocol of Figure 3 was $\sim 45\%$. For HeLa cells, minimal cytotoxicity was observed in the dark, even with porous Si nanoparticle concentrations as large as 100 $\mu\text{g}/\text{mL}$, indicating a low level of dark toxicity for the nanoparticles themselves. The morphology of HeLa cells exposed to 100 $\mu\text{g}/\text{mL}$ porous Si nanoparticles in the dark for 10 min, or with light exposure up to 60 J/cm^2 (100 mW/cm^2 , 10 min) but without nanoparticles, showed no significant change compared to an untreated control (Figure 4). However, under the same light exposure conditions, HeLa cells in the presence of porous Si nanoparticles lost their adherent nature and shrank to assume a spherical-like morphology (Figure 4d). Similar phototoxicity characteristics were observed using a blue ($\lambda_{\text{max}} = 458$ nm, $\text{fwhm} = 22$ nm) LED panel as the light source (Supporting Information, Figure S5a). The NIH-3T3 cells displayed qualitatively the same behavior, although they were more sensitive to the illumination protocol than HeLa cells; cytotoxicity associated with immersion in buffer and light irradiation was observed, even in the absence of Si nanoparticles (Figure 3b and Supporting Information,

Figure S5b). In addition, NIH-3T3 cells showed some dark toxicity at the largest nanoparticle concentration (100 $\mu\text{g}/\text{mL}$ porous Si nanoparticles). However, as was observed with the HeLa cells, the degree of

photoinduced cell death increased with increasing nanoparticle concentration.

A second illumination protocol was tested in which the nanoparticles and cells were irradiated in culture medium (RPMI-1640 medium without added FBS) rather than in buffer, and the nanoparticles were not removed with a postirradiation rinse but allowed to incubate with the cells for 24 h postirradiation (Figure 5). Both HeLa and NIH-3T3 cell lines required a significantly lower dose of light and silicon nanoparticles to achieve $\sim 45\%$ cell death with this protocol.

The increased degree of cell death observed in the experiments in which porous Si nanoparticles were irradiated in culture medium could be attributed to long-lived toxic species that are generated by the action of $^1\text{O}_2$ with organic species present in the vicinity of the nanoparticles during irradiation. This interpretation is consistent with prior studies on micrometer-sized particles of porous Si:⁴⁸ significant cell death was observed for microparticles incubated in cell culture medium for 24 h, and the authors of this prior work attributed the toxicity to persistent organic peroxides generated by the reaction of $^1\text{O}_2$ or other reactive oxygen species with amino acids such as tryptophan, histidine, and tyrosine.⁴⁸

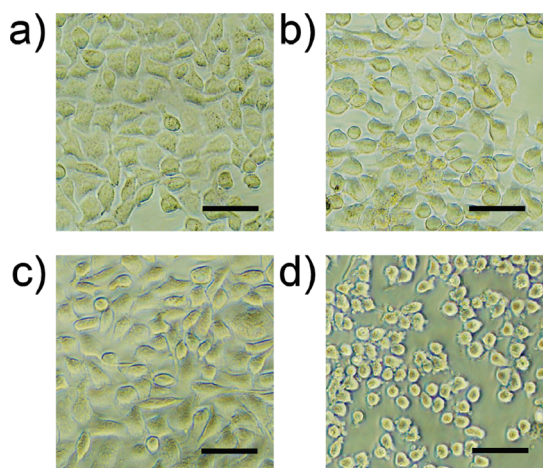


Figure 4. Phase contrast microscope images of HeLa cells treated with (a) PBS in the dark for 10 min (dark control), (b) 100 $\mu\text{g}/\text{mL}$ porous Si nanoparticles (PSiNP) in the dark for 10 min, (c) PBS under 60 J/cm^2 light irradiation for 10 min (light control), and (d) 100 $\mu\text{g}/\text{mL}$ PSiNP under 60 J/cm^2 light irradiation for 10 min. The scale bars are 50 μm .

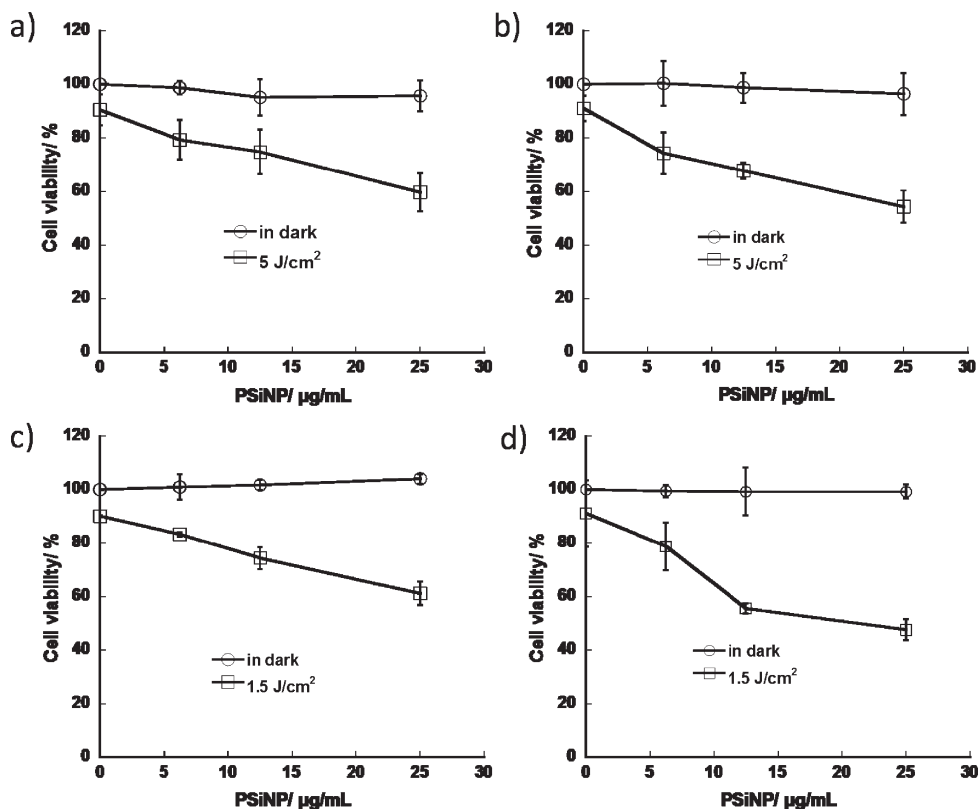


Figure 5. Phototoxicity exhibited by (a and c) HeLa cells and (b and d) NIH-3T3 cells treated with porous Si nanoparticles. In these experiments, the cells were not rinsed postirradiation as in Figure 3; instead, the cells were allowed to incubate with the nanoparticles in the culture medium for 24 h postirradiation. In panels a and b, the cells were irradiated with an (IR filtered) halogen lamp; in panels c and d, the cells were irradiated with a blue LED panel ($\lambda_{\text{max}} = 458 \text{ nm}$). The medium containing the porous Si nanoparticles was RPMI 1640 medium that did not contain FBS. Note the lower light flux and lower concentration of porous Si nanoparticles in this figure relative to that in Figure 3 and Figure S5. Cell viability was quantified by MTS assay. Each data point represents the mean of three independent experiments.

In comparison with a conventional PDT agent such as methylene blue, the porous Si nanoparticles are ~ 150 -fold less effective on a mass basis. Under the conditions of experiments in Figure 5, the 50% inhibitory concentration (IC_{50}) of methylene blue ($\Phi_{MB} = 0.39$ in PBS⁴⁰) was found to be $0.19 \mu\text{g/mL}$ for HeLa cells and $0.18 \mu\text{g/mL}$ for NIH-3T3 cells (24 h incubation after a 10-min application of 5 J/cm^2 light by IR-filtered halogen lamp, cells and nanoparticles in cell culture medium, no added FBS), compared to $\sim 30 \mu\text{g/mL}$ and $\sim 25 \mu\text{g/mL}$ for porous Si nanoparticles, respectively. The relatively low effectiveness of the porous Si nanoparticle system can be attributed to the relatively low quantum yield of $^1\text{O}_2$ generation in H_2O ($\Phi_{\text{PSINP}} = 0.17 \pm 0.01$), but it is also possible that dissolution of the porous Si nanoparticles in the cell culture medium during the course of the experiment plays a role. In separate experiments, we found that $\sim 54\%$ of the hydrogen-terminated porous Si nanoparticles degrade within 10 min at 37°C in RPMI-1640 medium without added FBS (Supporting Information, Figure S6). Photodegradation of the porous Si matrix may produce transient SiH_4 or other cytotoxic species that could contribute to cell death. The rapid degradation of the nanoparticles in buffer solutions places a limitation on PDT applications for the present nanoparticle formulation. The extent of degradation of the porous Si nanoparticles decreased to 32% when 10% FBS was present in the medium, although the addition of FBS was found to suppress the generation of $^1\text{O}_2$, as has been reported previously.⁴⁹ We attribute the increased stability of the porous Si nanoparticles in the presence of FBS to nonspecific adsorption of proteins on the nanoparticle surface. Much longer-lived nanoparticles based on oxidized porous Si have been developed, and their ability to image tumors in live animals has been demonstrated.³⁵ These latter Si-based nanoparticles contain a silica shell and they display strong photoluminescence (10% quantum yield).³⁵ However, the quantum yield for $^1\text{O}_2$ generation with this oxidized formulation under the conditions of the present experiments was $<3\%$.

It is worth noting that porous Si has also been proposed as an agent for cancer thermotherapy. Lee, *et al.* reported a marked photothermal effect by exposing porous Si to near-infrared light irradiation.⁵⁰ The possibility that the cell viability data presented in

this work result from photothermal (localized heating) effects rather than from photochemical ($^1\text{O}_2$ generation) effects was assessed by monitoring the local temperature in the culture medium during irradiation. In the absence of porous Si nanoparticles, application of the irradiation protocol used in the present work increased the temperature in the wells by 8.0°C or by 5.8°C for the IR-filtered tungsten-halogen or the LED source, respectively (Supporting Information, Figure S7a,b). In the presence of 0.1 mg/mL of porous Si nanoparticles (equal to the largest quantity used in the cell culture experiments), the temperature increase for the IR-filtered tungsten-halogen source was not distinguishable from the control, and the temperature increase for the LED source was 6.7°C , approximately 1°C warmer than the control. When a larger quantity of porous Si nanoparticles was present (6 mg/mL , in deionized water), a significant temperature rise (to 52°C) was observed, corresponding to 23°C greater than the control (Supporting Information, Figure S7c). Furthermore, if the irradiation power density on a sample containing 6 mg/mL of porous Si nanoparticles was increased to 300 mW/cm^2 , the temperature rise was 36°C greater than the control (Supporting Information, Figure S7d). Thus, although significant temperature increases can be obtained upon irradiation of porous Si nanoparticles in media, under the conditions of the cell culture experiments in the present work, the temperature rise is negligible.

In conclusion, porous Si nanoparticles function as intrinsic photosensitizers to generate measurable quantities of $^1\text{O}_2$. The measured quantum yield of $^1\text{O}_2$ by photoexcited porous Si nanoparticles was 0.10 ± 0.02 in ethanol and 0.17 ± 0.01 in H_2O . Porous Si nanoparticles irradiated with blue light show phototoxicity toward human HeLa and NIH-3T3 cancer cells *in vitro*. Although the porous Si nanoparticles used in this study are not as effective as conventional molecular PDT agents (based on IC_{50} values), they overcome some of their shortcomings: (1) the nanoparticles are not cytotoxic in the absence of light and (2) they degrade quickly to apparently nontoxic byproducts in buffer or culture media, minimizing the possibility of long-term patient photosensitivity. However, the rapid dissolution of the nanoparticle formulation used in this study limits its prospects for *in vivo* studies.

EXPERIMENTAL METHODS

Reagents. Boron-doped p-type Si wafers ($0.0008\text{--}0.0012 \Omega\text{-cm}$ resistivity, $\langle 100 \rangle$ orientation) were obtained from Siltronic. Aqueous hydrofluoric acid was purchased from EMD Chemicals. Methylene blue (MB), Rose Bengal (RB), and 1,3-diphenylisobenzofuran (DPBF) were obtained from Sigma-Aldrich Chemicals. Singlet oxygen sensor green (SOSG) reagent was purchased

from Molecular Probes, Inc. RPMI-1640 cell media, fetal bovine serum (FBS), trypsin, and Dulbecco's phosphate buffered saline (DPBS) were obtained from Thermo Scientific. CellTiter 96 Aqueous MTS Reagent Powder was purchased from Promega.

Preparation of Porous Si Nanoparticles. Porous Si nanoparticles were prepared by anodic electrochemical etch of Si in 3:1 (v/v) 48% aqueous HF/ethanol. A Teflon etch cell that exposed

8.8 cm² of the polished Si wafer surface was used. Samples were etched at a constant current density of 50, 100, 200, 300, or 400 mA/cm² for 150 s. The porous Si film was then removed from the crystalline Si substrate by application of a current pulse of 4 mA/cm² for 250 s in a solution of 3.3% aqueous HF in ethanol. The freestanding porous silicon film was fractured into nanoparticles by ultrasonication for ~16 h in ethanol under a nitrogen gas atmosphere. The large fragments were removed by filtration through a 0.45 μm nylon filter membrane (GE Osmonics Labstore). The porous Si nanoparticles were collected on a 100 kDa Amicon Ultra-4 membrane (Millipore) and washed three times with ethanol. FT-IR spectra were acquired using a Nicolet 6700 spectrometer equipped with a Smart-ATR attenuated total reflectance attachment.

Characterization of Porous Si Nanoparticles. Scanning electron microscope (SEM) images were obtained using a Philips XL30 field emission SEM. Dynamic light scattering (Zetasizer Nano ZS90, Malvern Instruments) was used to determine the hydrodynamic size of the porous Si nanoparticles.

Detection of Singlet Oxygen by Chemical Trapping. DPBF was used as a ¹O₂ trapping reagent in ethanol solution. In a typical experiment, 2 mL of an ethanol solution containing 0.08 mM DPBF and 10 μg/mL porous Si nanoparticles was placed in a sealed quartz cuvette. A 150 W tungsten halogen lamp (Fiber-Lite MI-150, Dolan-Jenner Industries) filtered through a short pass infrared and a bandpass filter (454–500 nm) was used as the light source. The absorbance of the solution at 410 nm was measured every 1 min for a 10 min period with an ultraviolet–visible spectrophotometer (SpectraMax Plus 384, Molecular Devices). The decrease of the absorbance caused by photobleaching of DPBF was measured and corrected in all experiments. The natural logarithm values of absorption of DPBF at 410 nm were plotted against the irradiation time and fit by a first-order linear least-squares model to get the decay rate of the photosensitized process. The ¹O₂ quantum yield of porous Si nanoparticles in ethanol was calculated using Rose Bengal as a standard (Φ_{RB} = 0.86 in ethanol⁴⁰). The ¹O₂ quantum yield of porous Si nanoparticles in aqueous solution was determined using the SOSG assay for ¹O₂; the fluorescence spectrum (LS50B spectrofluorimeter, Perkin-Elmer instruments) was integrated in the wavelength range from 500 to 570 nm for solutions containing 5 μM SOSG and 10 μg/mL PSiNP in water, using an excitation wavelength of 488 nm. The absolute quantum yield for ¹O₂ generation by porous Si nanoparticles in H₂O was calculated using Rose Bengal as a standard and assuming Φ_{RB} = 0.75 in H₂O.⁴⁰

In Vitro Degradation. A series of eight vials containing 0.02 mg/mL of porous Si nanoparticles in 1 mL PBS, RPMI-1640 medium, or RPMI-1640 medium with 10% FBS were incubated at 37 °C (porous Si nanoparticles incubated in water at 25 °C were used as control). At a given time point, one of the vials was removed from the pool of samples and subjected to silicon analysis. The silicon analysis was performed on 0.5 mL of the liquid, which was first filtered with a centrifugal filter (30K Da weight cutoff, Millipore) to remove the undissolved nanoparticles. The filtrate was then diluted with 2% aqueous HNO₃ and subjected to analysis by inductively coupled plasma optical emission spectroscopy (Optima 3000DV ICP-OES, Perkin-Elmer Instruments).

Cell Culture and In Vitro PDT. HeLa and Mouse embryonic fibroblast NIH 3T3 cell lines were cultured in RPMI 1640 medium supplemented with 10% fetal bovine serum (FBS) at 37 °C in a 5% CO₂ atmosphere. For *in vitro* PDT tests, the cells were seeded in 96-well plates at a density of 1 × 10⁴ cells/well and cultured for 24 h. An aliquot of 200 μL of PBS buffer containing 0, 25, 50, or 100 μg/mL of porous Si nanoparticles was injected, and immediately afterward the cells were exposed to a 150 W tungsten halogen lamp filtered with a short-pass infrared (IR) filter for 10 min at different intensities to apply a total light dose of 15, 45, or 60 J/cm². Alternatively, an LED panel (λ_{max} = 458 nm, fwhm = 22 nm) at a light dose of 6, 12, or 18 J/cm² was used. The control cells were maintained in the dark for the same period of time. After exposure, the buffer containing the nanoparticles was removed, the cells were washed twice with PBS solution, and they were then either subjected to cell viability assays or placed under the microscope for observation of morphology. For the cell viability experiments, the plates were further

incubated in RPMI 1640 medium supplemented with 10% FBS for 24 h and assayed using the CellTiter 96 Aqueous One Solution Cell Proliferation (MTS) assay according to the instructions provided by the vendor. In a second protocol, the porous Si nanoparticles were suspended in 200 μL of RPMI 1640 medium (with no added FBS) and added to the culture plates as described above, but the porous Si nanoparticles were not removed and the cells were not washed with PBS after irradiation. The cells were then incubated and subjected to MTS assay as described above, 24 h postirradiation. Smaller doses of porous Si nanoparticles (0, 6.25, 12.5, 25 μg/mL) and lower light doses (5 J/cm² IR-filtered halogen lamp or 1.5 J/cm² LED lamp) were applied in this set of experiments. Each experiment was repeated three times independently.

Temperature Measurements of Porous Si Nanoparticles Undergoing Irradiation. One mL solutions of RPMI-1640 medium supplemented with 10% FBS and containing 0.1 or 6 mg/mL porous Si nanoparticles were exposed to a tungsten halogen lamp (100 or 300 mW/cm²) filtered with a short-pass infrared (IR) filter or a blue LED lamp (λ_{max} = 458 nm, fwhm = 22 nm, 30 mW/cm²) continuously for 10 min. Media that contained no porous Si nanoparticles were irradiated under the same conditions as controls for each group. The temperature of each solution was recorded by means of an *in situ* thermocouple probe at intervals of 1 min using an OMEGA HH309A thermometer/data logger.

Acknowledgment. This material is based upon work supported by the National Science Foundation under Grant No. DMR-0806859 and by the National Institutes of Health (NIH) Grant 5-R01-CA124427. L. Xiao acknowledges support from the China Scholarship Council (CSC).

Supporting Information Available: Schematic diagram of the preparation of porous Si nanoparticles, FT-IR spectrum of porous Si nanoparticles, decomposition of DPBF in the absence of porous Si nanoparticles (with and without N₂ purge), DPBF-based quantification of singlet oxygen generation for different amounts of porous Si nanoparticles in ethanol, SOSG-based quantification of singlet oxygen generation for porous Si nanoparticles in H₂O, phototoxicity of HeLa and NIH-3T3 cells by porous Si nanoparticles irradiated with LED panel, and ICP–MS-based quantification of degradation of porous Si nanoparticles in RPMI-1640 medium (with and without 10% FBS), PBS and H₂O. This material is available free of charge via the Internet at: <http://pubs.acs.org>.

REFERENCES AND NOTES

- Sharman, W. M.; Allen, C. M.; Van Lier, J. E. Photodynamic Therapeutics: Basic Principles and Clinical Applications. *Drug Discovery Today* **1999**, *4*, 507–517.
- Dougherty, T. J.; Gomer, C. J.; Henderson, B. W.; Jori, G.; Kessel, D.; Korbelik, M.; Moan, J.; Peng, Q. Photodynamic Therapy. *J. Natl. Cancer Inst.* **1998**, *90*, 889–905.
- Dolmans, D. E.; Fukumura, D.; Jain, R. K. Photodynamic Therapy for Cancer. *Nat. Rev. Cancer* **2003**, *3*, 380–387.
- Sibata, C. H.; Colussi, V. C.; Oleinick, N. L.; Kinsella, T. J. Photodynamic Therapy in Oncology. *Expert Opin. Pharmacother.* **2001**, *2*, 917–927.
- Allison, R. R.; Downie, G. H.; Cuenca, R.; Hu, X.-H.; Childs, C. J. H.; Sibata, C. H. Photosensitizers in Clinical PDT. *Photodiagn. Photodyn. Ther.* **2004**, *1*, 27–42.
- Allen, C. M.; Sharman, W. M.; Van Lier, J. E. Current Status of Phthalocyanines in the Photodynamic Therapy of Cancer. *J. Porphyrins Phthalocyanines* **2001**, *5*, 161–169.
- Zharkova, N. N.; Sokolov, V. V.; Chissov, V. I.; Aristarkhova, E. I.; Kozlov, D. N.; Smirnov, V. V. Fluorescence Examinations of Patients with Tumors of Different Localizations in the Course of Photodynamic Therapy with Photosensitizer Photosens. In *Photochemotherapy: Photodynamic Therapy and Other Modalities*; Benjamin, E., Giulio, J., Johan, M., Eds.; SPIE Publications, 1995; Proceedings Volume, pp 476–481.
- Josefsen, L. B.; Boyle, R. W. Photodynamic Therapy: Novel Third-Generation Photosensitizers One Step Closer?. *Br. J. Pharmacol.* **2008**, *154*, 1–3.

9. Bechet, D.; Couleaud, P.; Frochet, C.; Viriot, M. L.; Guillemin, F.; Barberi-Heyob, M. Nanoparticles as Vehicles for Delivery of Photodynamic Therapy Agents. *Trends Biotechnol.* **2008**, *26*, 612–621.
10. Wang, S. Z.; Gao, R. M.; Zhou, F. M.; Selke, M. Nanomaterials and Singlet Oxygen Photosensitizers: Potential Applications in Photodynamic Therapy. *J. Mater. Chem.* **2004**, *14*, 487–493.
11. Zhao, B. Z.; Yin, J. J.; Bilski, P. J.; Chignell, C. F.; Roberts, J. E.; He, Y. Y. Enhanced Photodynamic Efficacy towards Melanoma Cells by Encapsulation of Pc4 in Silica Nanoparticles. *Toxicol. Appl. Pharmacol.* **2009**, *241*, 163–172.
12. Ohulchanskyy, T. Y.; Roy, I.; Goswami, L. N.; Chen, Y.; Bergey, E. J.; Pandey, R. K.; Oseroff, A. R.; Prasad, P. N. Organically Modified Silica Nanoparticles with Covalently Incorporated Photosensitizer for Photodynamic Therapy of Cancer. *Nano Lett.* **2007**, *7*, 2835–2842.
13. He, X. X.; Wu, X.; Wang, K. M.; Shi, B. H.; Hai, L. Methylene Blue-Encapsulated Phosphonate-Terminated Silica Nanoparticles for Simultaneous *In Vivo* Imaging and Photodynamic Therapy. *Biomaterials* **2009**, *30*, 5601–5609.
14. Tu, H. L.; Lin, Y. S.; Lin, H. Y.; Hung, Y.; Lo, L. W.; Chen, Y. F.; Mou, C. Y. *In Vitro* Studies of Functionalized Mesoporous Silica Nanoparticles for Photodynamic Therapy. *Adv. Mater.* **2009**, *21*, 172–177.
15. Jang, W. D.; Nishiyama, N.; Zhang, G. D.; Harada, A.; Jiang, D. L.; Kawachi, S.; Morimoto, Y.; Kikuchi, M.; Koyama, H.; Aida, T.; *et al.* Supramolecular Nanocarrier of Anionic Dendrimer Porphyrins with Cationic Block Copolymers Modified with Polyethylene Glycol to Enhance Intracellular Photodynamic Efficacy. *Angew. Chem., Int. Ed.* **2005**, *44*, 419–423.
16. Naito, K.; Tachikawa, T.; Cui, S. C.; Sugimoto, A.; Fujitsuka, M.; Majima, T. Single-Molecule Detection of Airborne Singlet Oxygen. *J. Am. Chem. Soc.* **2006**, *128*, 16430–16431.
17. Daimon, T.; Nosaka, Y. Formation and Behavior of Singlet Molecular Oxygen in TiO₂ Photocatalysis Studied by Detection of Near-Infrared Phosphorescence. *J. Phys. Chem. C* **2007**, *111*, 4420–4424.
18. Juzenas, P.; Chen, W.; Sun, Y. P.; Coelho, M. A.; Generalov, R.; Generalova, N.; Christensen, I. L. Quantum Dots and Nanoparticles for Photodynamic and Radiation Therapies of Cancer. *Adv. Drug Delivery Rev.* **2008**, *60*, 1600–1614.
19. Samia, A. C.; Chen, X.; Burda, C. Semiconductor Quantum Dots for Photodynamic Therapy. *J. Am. Chem. Soc.* **2003**, *125*, 15736–15737.
20. Wang, J. X.; Liu, Y.; Jiao, F.; Lao, F.; Li, W.; Gu, Y. Q.; Li, Y. F.; Ge, C. C.; Zhou, G. Q.; Li, B.; *et al.* Time-Dependent Translocation and Potential Impairment on Central Nervous System by Intranasally Instilled TiO₂ Nanoparticles. *Toxicology* **2008**, *254*, 82–90.
21. Warheit, D. B.; Webb, T. R.; Sayes, C. M.; Colvin, V. L.; Reed, K. L. Pulmonary Instillation Studies with Nanoscale TiO₂ Rods and Dots in Rats: Toxicity Is Not Dependent upon Particle Size and Surface Area. *Toxicol. Sci.* **2006**, *91*, 227–236.
22. Wu, J. H.; Liu, W.; Xue, C. B.; Zhou, S. C.; Lan, F. L.; Bi, L.; Xu, H. B.; Yang, X. L.; Zeng, F. D. Toxicity and Penetration of TiO₂ Nanoparticles in Hairless Mice and Porcine Skin after Subchronic Dermal Exposure. *Toxicol. Lett.* **2009**, *191*, 1–8.
23. Hardman, R. A Toxicologic Review of Quantum Dots: Toxicity Depends on Physicochemical and Environmental Factors. *Environ. Health Perspect.* **2006**, *114*, 165–172.
24. Bakalova, R.; Ohba, H.; Zhelev, Z.; Ishikawa, M.; Baba, Y. Quantum Dots as Photosensitizers?. *Nat. Biotechnol.* **2004**, *22*, 1360–1361.
25. Fujii, M.; Minobe, S.; Usui, M.; Hayashi, S.; Gross, E.; Diener, J.; Kovalev, D. Generation of Singlet Oxygen at Room Temperature Mediated by Energy Transfer from Photoexcited Porous Si. *Phys. Rev. B* **2004**, *70*, 085311.
26. Kovalev, D.; Fujii, M. Silicon Nanocrystals: Photosensitizer for Oxygen Molecules. *Adv. Mater.* **2005**, *17*, 2531–2544.
27. Bayliss, S. C.; Buckberry, L. D.; Harris, P. J.; Tobin, M. Nature of the Silicon–Animal Cell Interface. *J. Porous Mater.* **2000**, *7*, 191–195.
28. Foraker, A. B.; Walczak, R. J.; Cohen, M. H.; Boiarski, T. A.; Grove, C. F.; Swaan, P. W. Microfabricated Porous Silicon Particles Enhance Paracellular Delivery of Insulin across Intestinal Caco-2 Cell Monolayers. *Pharm. Res.* **2003**, *20*, 110–116.
29. Canham, L. T. Bioactive Silicon Structure Fabrication through Nanoetching Techniques. *Adv. Mater.* **1995**, *7*, 1033–1037.
30. Canham, L. T. Porous Silicon as a Therapeutic Biomaterial. In *Microtechnologies in Medicine and Biology*, 1st Annual International Conference; Lyon, France, October 12–14, 2000; pp 109–112.
31. Low, S. P.; Voelcker, N. H.; Canham, L. T.; Williams, K. A. The Biocompatibility of Porous Silicon in Tissues of the Eye. *Biomaterials* **2009**, *30*, 2873–2880.
32. Jugdaohsingh, R. Silicon and Bone Health. *J. Nutr., Health Aging* **2007**, *11*, 99–110.
33. Mertz, W. The Essential Trace Elements. *Science* **1981**, *213*, 1332–1338.
34. Yoo, Y. C.; Lee, S. K.; Yang, J. Y.; In, S. W.; Kima, K. W.; Chung, K. H.; Chung, M. G.; Choung, S. Y. Organ Distribution of Heavy Metals in Autopsy Material from Normal Korean. *J. Health Sci.* **2002**, *48*, 186–194.
35. Park, J. H.; Gu, L.; Von Maltzahn, G.; Ruoslahti, E.; Bhatia, S. N.; Sailor, M. J. Biodegradable Luminescent Porous Silicon Nanoparticles for *In Vivo* Applications. *Nat. Mater.* **2009**, *8*, 331–336.
36. Howard, J. A.; Mendenhall, G. D. Autoxidation and Photooxidation of 1,3-Diphenylisobenzofuran: A Kinetic and Product Study. *Can. J. Chem.* **1975**, *53*, 2199–2201.
37. Fujii, M.; Usui, M.; Hayashi, S.; Gross, E.; Kovalev, D.; Kunzner, N.; Diener, J.; Timoshenko, V. Y. Chemical Reaction Mediated by Excited States of Si Nanocrystals—Singlet Oxygen Formation in Solution. *J. Appl. Phys.* **2004**, *95*, 3689–3693.
38. Hoebeke, M.; Damoiseau, X. Determination of the Singlet Oxygen Quantum Yield of Bacteriochlorin a: A Comparative Study in Phosphate Buffer and Aqueous Dispersion of Dimiristoyl-L- α -Phosphatidylcholine Liposomes. *Photochem. Photobiol. Sci.* **2002**, *1*, 283–287.
39. Venkatesan, R.; Periasamy, N.; Srivastava, T. S. Singlet Molecular-Oxygen Quantum Yield Measurements of Some Porphyrins and Metalloporphyrins. *Proc. Indian Acad. Sci. Chem. Sci.* **1992**, *104*, 713–722.
40. Redmond, R. W.; Gamlin, J. N. A Compilation of Singlet Oxygen Yields from Biologically Relevant Molecules. *Photochem. Photobiol.* **1999**, *70*, 391–475.
41. Timoshenko, V. Light-Induced Generation of Singlet Oxygen in Porous Silicon. In *Sensors for Environment, Health and Security*; Baraton, M. I., Ed.; Springer: The Netherlands, 2009; pp 125–139.
42. Hurst, J. R.; Schuster, G. B. Nonradiative Relaxation of Singlet Oxygen in Solution. *J. Am. Chem. Soc.* **1983**, *105*, 5756–5760.
43. Ghulinyan, M.; Gelloz, B.; Ohta, T.; Pavesi, L.; Lockwood, D. J.; Koshida, N. Stabilized Porous Silicon Optical Superlattices with Controlled Surface Passivation. *Appl. Phys. Lett.* **2008**, *93*, 061113.
44. Fujii, M.; Nishimura, N.; Fumon, H.; Hayashi, S.; Kovalev, D.; Goller, B.; Diener, J. Dynamics of Photosensitized Formation of Singlet Oxygen by Porous Silicon in Aqueous Solution. *J. Appl. Phys.* **2006**, *100*, 124302.
45. Flors, C.; Fryer, M. J.; Waring, J.; Reeder, B.; Bechtold, U.; Mullineaux, P. M.; Nonell, S.; Wilson, M. T.; Baker, N. R. Imaging the Production of Singlet Oxygen *In Vivo* Using a New Fluorescent Sensor, Singlet Oxygen Sensor Green. *J. Exp. Bot.* **2006**, *57*, 1725–1734.
46. Ragàs, X.; Jiménez-Banzo, A.; Sánchez-García, D.; Batllori, X.; Nonell, S. Singlet Oxygen Photosensitisation by the Fluorescent Probe Singlet Oxygen Sensor Green. *Chem. Commun.* **2009**, 2920–2922.
47. Yan, F.; Zhang, Y.; Kim, K. S.; Yuan, H. K.; Vo-Dinh, T. Cellular Uptake and Photodynamic Activity of Protein Nanocages Containing Methylene Blue Photosensitizing Drug. *Photochem. Photobiol.* **2010**, *86*, 662–666.

48. Low, S. P.; Williams, K. A.; Canham, L. T.; Voelcker, N. H. Generation of Reactive Oxygen Species from Porous Silicon Microparticles in Cell Culture Medium. *J. Biomed. Mater. Res. A* **2010**, *93A*, 1124–1131.
49. Lee, S.; Zhu, L. Y.; Minhaj, A. M.; Hinds, M. F.; Vu, D. H.; Rosen, D. I.; Davis, S. J.; Hasan, T. Pulsed Diode Laser-Based Monitor for Singlet Molecular Oxygen. *J. Biomed. Opt.* **2008**, *13*, 034010.
50. Lee, C.; Kim, H.; Hong, C.; Kim, M.; Hong, S. S.; Lee, D. H.; Lee, W. I. Porous Silicon as an Agent for Cancer Thermotherapy Based on Near-Infrared Light Irradiation. *J. Mater. Chem.* **2008**, *18*, 4790–4795.